

A Quasi oppositional smell agent optimization and its levy flight variant: A PV/Wind/battery system optimization application

Abdullahi Abubakar Mas'ud^{a*}, Ahmed T. Salawudeen^b, Abubakar Ahmad Umar^c, Ali Saleh Aziz^d, Yusuf A. Shaaban^e, Firdaus Muhammad-Sukki^{f,g,h*}, Umar Musa^c

^a Department of Electrical Engineering, Jubail Industrial College, Royal commission for Jubail, Saudi Arabia.

^b Department of Electrical and Electronic Engineering, University of Jos, Nigeria.

^c Department of Electrical Engineering, Ahmadu Bello University, Samaru, Zaria, Nigeria.

^d Department of Electrical Power Techniques Engineering, Al-Hussain University College, 56001, Karbala, Iraq

^e Department of Electrical Engineering, University of Hafr Batin, Saudi Arabia.

^f School of Computing, Engineering and the Built Environment, Edinburgh Napier University, Merchiston Campus, 10 Colinton Road, Edinburgh EH10 5DT, Scotland, UK.

^g Razak Faculty of Technology and Informatics, Universiti Teknologi Malaysia, Jalan Sultan Yahya Petra, Kuala Lumpur 54100, Malaysia.

^h Solar Research Institute (SRI), School of Electrical Engineering, College of Engineering, Universiti Teknologi MARA (UiTM), Shah Alam 40450, Malaysia

*Corresponding author: masud_a@rcjy.edu.sa (A.A.M); f.muhammadsukki@napier.ac.uk (F.M.-S)

Abstract: In this study, two novel algorithms are developed: the quasi oppositional smell agent optimization (QOBL-SAO) and its levy flight variation (LFQOBL-SAO), and their performance is compared to that of the conventional smell agent optimization (SAO). Two investigations were carried out. First, the capabilities of the novel algorithms were tested in solving ten benchmarked functions and five CEC2020 real world optimization problems. Second, they are applied to optimize the hybrid photovoltaic (PV)/wind/battery, PV/battery and wind/battery power system for a healthcare centre in a Nigerian village. Load demand, PV and wind profiles of the aforementioned location were used to developed the hybrid system. All simulations were carried out in MATLAB software and the results show that the novel algorithms are capable of solving both the benchmarked functions and the CEC2020 real world constrained optimization competition. In particular, the performance of the QOBL and the LF-QOBL are as good as the top performing functions like the IUDE, ϵ MAGES and the iLSHADE algorithms. However, in terms of convergence time, lowest cost of energy (LCE), and total annualized cost (TAC), the novel algorithms outperformed the SAO for the PV/wind/battery optimization application. The hybrid PV/wind/battery system is the most cost-effective when using LFQOBL-SAO and QOBL-SAO, with a TAC value of \$15100. Furthermore, the results demonstrate that the LFQOBL-SAO method is accurate and outperforms the QOBL-SAO and SAO algorithms.

Keywords: Quasi oppositional smell agent optimization, levy flight quasi oppositional smell agent optimization, smell agent optimization, photovoltaic, wind, renewable energy sources, lowest cost of energy, net present cost and hybrid system.

1. Introduction

Greenhouse gas (GHG) emissions have attracted the attention of this generation, which is increasingly focused on harnessing renewable energy sources (RES) as a result of technological advancement, population growth, and compelling evidence of the global warming phenomenon. [1][2]. RES has been identified as a viable power supply solution in isolated and remote locations where the utility grid is unavailable [3,4]. RES includes wind, solar, biomass, geothermal, and other natural resources. These energy sources are considered the most plentiful because they can be found almost anywhere on the planet and may never run out, but, they are also the most unpredictable [5][6]. In contrast to fossil fuels, most RES are intermittent and are influenced by the weather, negatively affecting energy production. In order to address this issue, RES can be combined with other conventional sources and an energy storage system to provide a more reliable source of energy. Unexpected increases in load demand within the system can also be accommodated by combining these RES in a hybrid form [7][8].

Hybrid RES (HRES) have been the subject of several research investigations throughout the years in many regions of the world [9–18]. Specifically, Zhang et al. [9] utilized the hybrid optimization model for electric renewables (HOMER), to develop a unique optimum configuration of an HRES to fulfil the necessary electrical power demand of a medium-size workshop in an industrial district of Ardabil, Iran. The result showed that a storage bank consisting of a 1 kW photovoltaic (PV) array, 6.13 kW converter, 27 strings of 1 kW batteries, 13 kW diesel generator (DG) and two 3 kW wind turbines is the optimal option for obtaining a levelized cost of Energy (LCE) of 0.462 \$/kWh in the Ardabil region. However, the work was characterized by high excess energy and GHG emissions due to a DG in the system. In another study, Izadyar et al. [19] utilized HOMER to evaluate the techno-economics of deploying HRES to identify the most promising sources and regions for deployment in Malaysia. With a net present cost (NPC) of \$696,083, the results show that Langkawi was suitable for deploying solar or wind power stations, while Tioman is more suitable for HRES installations. With regards to an HRES optimization using artificial intelligence, a more recent work by Bhimaraju et al. [17], optimized a hybrid PV/wind//battery system using the teaching learning based optimization (TLBO) algorithm. The hybrid system minimized energy and Loss of Power Supply Probability (LPSP) costs in Kanyakumari, India, for optimal sizing scheme. The results showed that the TLBO, with LCE of 0.2104 \$/kWh and LPSP of 0.0498, provided the best hybrid system configuration and converged more quickly than the other algorithms. Additionally, Fu et.al [18] developed an improved PSO to adjust the PSO parameters based on the differential evolutionary algorithm. All simulations were performed in MATLAB, and the results showed that the PSO method required 400kWh of battery capacity for a

system with 100kW PV and 100kW wind generation, but this improved technique only requires 330kWh. Generally, most of the recent optimization techniques for hybrid RE systems are based on improving an existing algorithm with very little improvement in some cases which might not have any economic impact.

Nigeria, on the other hand, is one country which has an abundance of underutilized RES. The country lies between 3° and 14° east of Greenwich and 4° and 14° north of the equator[20]. The year-round climate is favourable for wind and solar energy generation which offers the best solutions for meeting current and future power system developments in rural communities [21]. However, hydropower is the only RES currently being used and connected to the grid [22]. Based on the report from the International Energy Agency, electricity is accessible to only 10% of rural communities and approximately 30% of Nigeria's total population do not have access to electricity [23]. Inadequate infrastructure and insufficient pricing structure to support the economics of power generation, transmission, and distribution are the main obstacles to Nigeria's safe and efficient electricity supply. The government has planned to include RES in its future power generation options. According to Nigeria's renewable energy master plan, renewable electricity generation is expected to reach 36% by 2030. Few studies carried out a feasibility study on the application of HRES for some locations in Nigeria. Olatomiwa et al. [24] used HOMER to analyse various power generation configurations in different locations across Nigeria's six geopolitical zones. The PV/diesel/battery scheme was the best, with the lowest cost, less fuel consumption and low CO₂ emission. Babatunde et al. [25] presented an optimal HRES for rural healthcare in Nigeria. Across all locations studied, the PV/diesel/battery system appears to be the best option, with the NPC and renewable fraction ranging from \$12,779 to \$13,646 and 70% to 80%, respectively. The LCE is within the range of \$0.507-0.542 /kWh. Most of the research for off-grid renewable energy systems concentrates on PV/diesel only system. While previous research has identified good locations for wind power generation in Nigeria [26], HRES that take advantage of both solar and wind power have received comparatively little attention. Also, little or no research has been done to develop an HRES comprising PV and wind for a healthcare facility in the northwestern region of Nigeria, an area known for its high solar and wind energy resources.

Recently, Salawuddeen et al. [27] developed a novel smell agent optimization (SAO) for engineering problems related to the HRES. The SAO can provide a cost-effective scheme as compared to other algorithms. In this study, two modified versions of the SAO were developed, and the results were compared with the conventional SAO. The two modified versions are Quasi-oppositional based learning (QOBL-SAO) and the levy flight quasi-oppositional-based learning (LFQOBL-SAO). The techno-economic design of a HRES for power generation

considering a healthcare facility in Jibia, Nigeria, will be investigated. The aforementioned location was chosen because of its high wind and solar energy potentials.

The outline for the paper is as follows: Section 1 introduces the research while Section 2 presents the methodology employed in achieving the research objectives. In Section 3, the implementation of the optimum HRES based on the QOBL-SAO and LFQOBL-SAO are presented. Subsequently, Section 4 presents the evaluation criteria for the QOBL-SAO and LFQOBL-SAO. Section 5 shows the analysis of the benchmarked functions, Section 6 is the results and analysis section and Section 7 concludes the paper.

2.0 Methodology

This section describes the study's methodology. The wind, solar and temperature profiles of a given location are required to evaluate which energy system option is technically and economically viable. In order to calculate the appropriate size of the energy system and its cost implications, the average power demand of the community is also required.

2.1 Site location and the load profile

The healthcare centre under study, was established in 1997. It is situated in Jibia, Nigeria with coordinates 13.0931°N, 7.2248°E. It's electrical consumption comprises a number of components including heating, air conditioning, biomedical equipment and kitchen utensils. Figure 1 shows the average daily load profile of the centre. The data was obtained from Nigeria's power holding company and is based on the location's average annual energy consumption over a three-year period (see Figure 2) [28]. Due to the high energy demand of the cooling units, the summer seasons have the highest electricity demand. It can be observed that, on average, the highest load consumption is around 22 kW at 19:00 hrs. This is due to the hospital's regular activities in the clinical and administrative blocks.

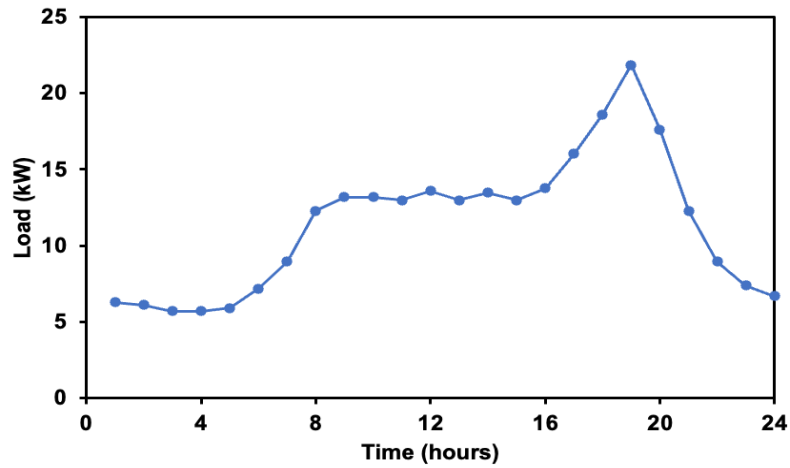


Figure 1: The mean daily load profile of the Hospital.

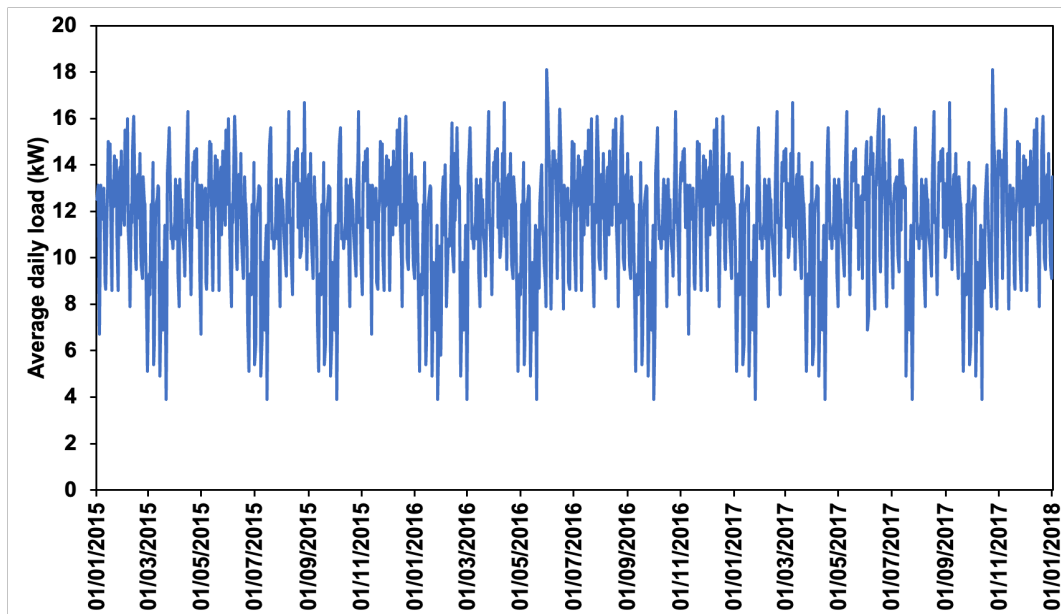


Figure 2: Three-year load profile of the healthcare centre (2015-2018).

2.2 Wind and solar resource assessment

The monthly solar irradiation of Jibia town, where the health care facility was located, is depicted in Figure 3 [29]. The months with the highest and lowest mean solar radiation values are March (312 W/m^2) and August (235 W/m^2), respectively. The ambient temperature of the location under study is critical in determining the actual power production of the solar PV panels. Figure 4 depicts the monthly average of Jibia's ambient temperature. In addition, the highest and lowest ambient temperatures appear in May and August, respectively. It can be inferred that ambient temperature does have a negative impact on solar PV efficiency. Jibia has a mean wind speed of 6.3 m/s , which is considered sufficient for power generation. Throughout the year, the average monthly wind speed

ranges between 4-9 m/s. The average wind speed in August is 4.65 m/s, while the average wind speed in January is 8.5 m/s.. The wind speed profile for Jibia is shown in Figure 5.

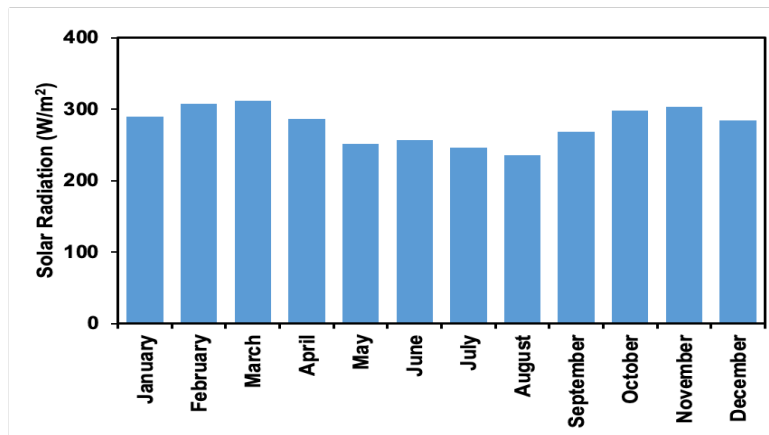


Figure 3: Jibia's monthly solar radiation pattern

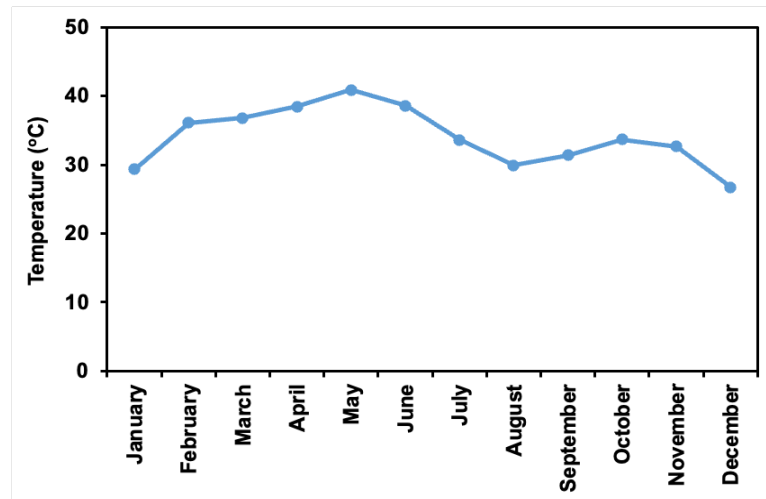


Figure 4: Monthly ambient temperature for Jibia.

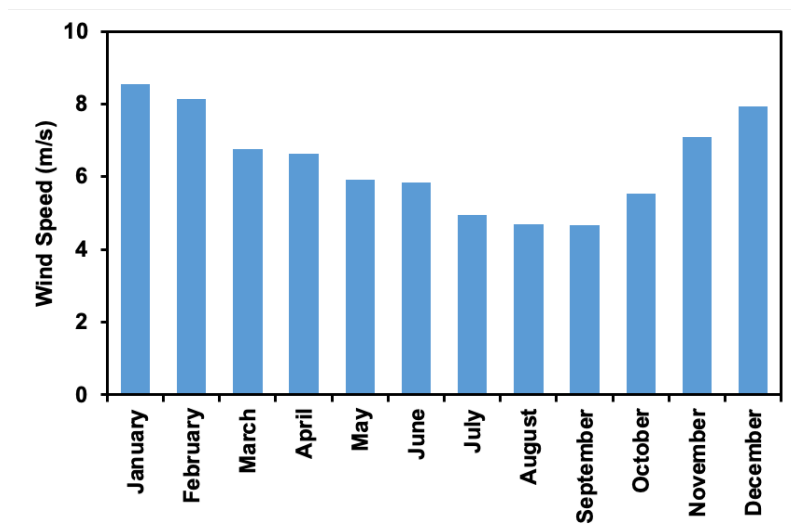


Figure 5: Jibia's Wind Speed Data

2.2 Formulation of the PV/Wind/Battery Scheme

In this study, the HRES comprises a battery storage system, wind turbine generator and a PV. Figure 6 is a schematic diagram of the HRES, and Table 1 shows the technical specifications of the components.

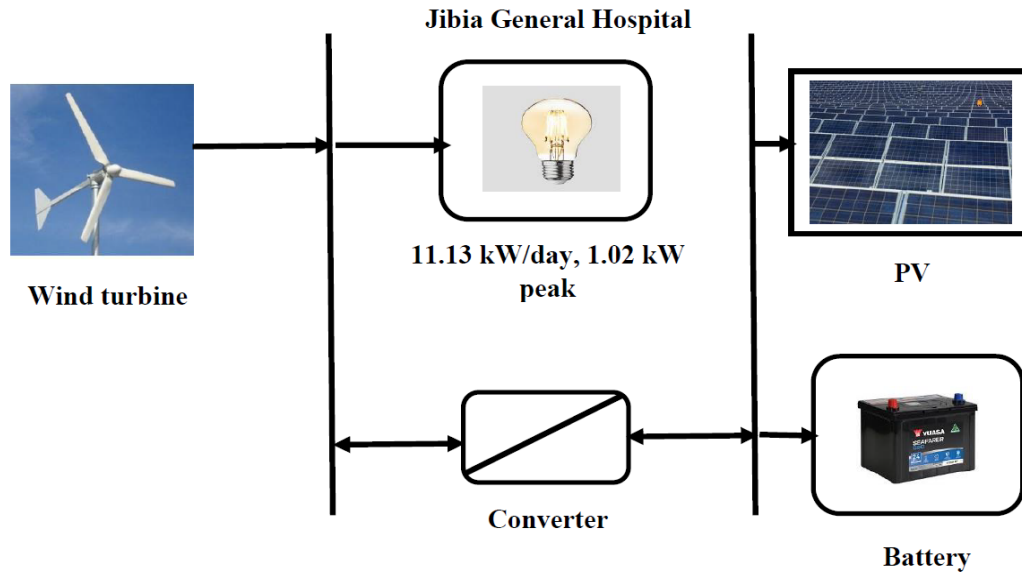


Figure 6: Schematic diagram of the HRES for Jibia

Table 1: Components of the hybrid renewable energy schemes and their specifications

Component	Parameters	Specifications
Wind Turbine	Capital cost	\$1250/kW
	Lifetime	15 years
	Replacement cost	\$1250/kW
	Cut-out speed	25 m/s
	Hub height	20 m
	Operation and maintenance cost	\$50/year
	Model	Venturi 1 kW
	Cut-in speed	2 m/s
PV	Capital cost	\$240/kW
	PV efficiency	15.7%
	Model	Generic flat plate PV
	Replacement cost	\$240/kW
	Lifetime	25 years
Converter	Operation and maintenance cost	\$15/year
	Capital cost	\$2000
	Lifetime	15 years
	Replacement cost	\$2000
Batteries	Operation and maintenance cost of the converter	\$15/year
	Nominal capacity	2.4 kWh
	Model	Lead acid
	Battery depth of discharge	0.8

	Capital cost	\$350
	Replacement cost	\$350
	Nominal voltage	12V
	Operating and maintenance cost	\$25/year

2.2.1 PV array

The performance of the HRES is evaluated using a recursive procedure that terminates when the optimal configuration is achieved. The area of the PV module is determined using Equation (1)[30]:

$$A_{PV} = \frac{E_L}{H_{t(av)} \times \eta_{pv} \times \eta_{batt} \times \eta_{conv} \times A_{tcf}} \quad (1)$$

where A_{PV} is the PV modules area required to meet the load demand, E_L = Estimated daily energy demand, $H_{t(av)}$ = mean global solar radiation of the area, η_{pv} = PV efficiency, η_{batt} =Battery efficiency, η_{conv} = Converter efficiency and A_{tcf} =Temperature correction factor.

The estimated solar energy required for the load demand can be determined by calculating the amount of PV module required using Equation (2):

$$\eta_{pv} = \frac{P_{PV}}{S_p} \quad (2)$$

where S_p =peak power of the chosen PV module based on the manufacturer's dataset, P_{PV} is the PV module's output power.

2.2.2 Wind turbine power

The instantaneous wind speed, v , as a function of the available wind generator output power is described in Equation (3)[31]:

$$P_{wind} = \begin{cases} 0 & v < v_{ci} \\ p_r \left(\frac{v^3 - v_{ci}^3}{v_r^3 - v_{ci}^3} \right), & v_{ci} < v < v_r \\ p_r & v_r < v < v_{co} \\ 0 & v > v_{co} \end{cases} \quad (3)$$

where v_{ci} is the cut-in wind speed, P_r is the rated electrical power, v_{co} is the cut-out wind speed and v_r is the rated wind speed. The following equation (4) can be used to determine the size of the wind turbines[31]:

$$N_{wt} = \frac{P_L \times SF}{P_{wt}} \quad (4)$$

where: SF is the safety factor, usually 120%, P_{wt} is the output power of the wind and P_L is the consumers load demand.

2.2.3 Battery bank model

The battery stores energy and balance the electrical power between the supply and the demand [32][33]. The battery system's required Ampere-hour (Ah) is calculated using Equation (5) [34].

$$M_{batt} = \frac{Ad \times El}{\eta_{batt} \times \eta_{inv} \times DoD \times V_s} \quad (5)$$

where Ad denotes the autonomous days of the battery, El is the unceasing energy that never has to be recharged by a power source, DoD stands for the maximum allowable depth of discharge and V_s is the voltage of the battery.

Equation 6 can be used to determine the number of batteries required by the system.

$$\eta_{batt} = \frac{M_{batt}}{M_{sin}} \quad (6)$$

where M_{sin} is the battery's storage capacity in Ah.

2.2.3.1 The Battery state of charge

The battery's current state of charge is expressed as SOC(t), where t is the battery's charge level at a specified time t . It is constrained by $SOC_{min} \leq SOC(t) \leq SOC_{max}$, where SOC_{min} and SOC_{max} are the minimum and maximum charge level of the battery storage system respectively. It depends on the DoD; i.e. $SOC_{min} = (1-DoD) \cdot CB$. At the peak charge, $SOC(t) = SOC_{max} - CB$ [34]. CB is the battery's nominal capacity.

The battery's average energy capacity can be calculated using Equations (7) and (8) [35].

$$P_{batt} = E_g - P_{Load} \quad (7)$$

$$A_E = A_{EO} - \sum_{t1}^{t2} \frac{P_{batt}}{V_{batt}} \quad (8)$$

where: P_{batt} = Power flow in and out of the battery, E_g = Generated power from PV and Wind, P_{Load} = Load power, A_E = average energy capacity, A_{EO} = initial state of the battery and V_{batt} = Battery voltage.

2.3 The Smell Agent Optimization

The SAO belongs to the class of swarm intelligence paradigm [27]. The optimization procedures of SAO are inspired by the conception that an agent has the aptitude to trail part of a smell molecule using the chemosensory

receptors of the olfactory organ. This aptitude is modelled into three distinctive phases: sniffing, random and trailing modes. The idea that the smell molecules must spread in the direction of the agent according to the hydrostatic gas theory inspired the sniffing mode [36]. Detail description of the three phases of the SAO is highlighted as follows:

2.3.1 Sniffing mode

The SAO heavily relies on smell molecules evaporating toward an agent's fixed location. This evaporation is initiated by randomly creating an initial population of smell molecules. Assuming that initialization of population ($nPop$) is the number of nominee solutions of smell molecules, and the problem dimension ($nVar$) denotes the control variables in the optimization hyperspace, then the current population of smell molecules can be formulated using Equation (9).

$$n_i^{(t)} = \begin{bmatrix} n_{(1,1)} & \cdots & n_{(1,j)} & n_{(1,nVar-1)} & n_{(1,nVar)} \\ n_{(2,1)} & \cdots & n_{(2,j)} & \cdots & n_{(2,nVar)} \\ \cdots & \cdots & n_{(i,j)} & \cdots & \cdots \\ \vdots & \vdots & \vdots & \vdots & \vdots \\ n_{(nPop-1,1)} & \cdots & n_{(nPop-1,j)} & \cdots & n_{(nPop-1,nVar)} \\ n_{(nPop,1)} & \cdots & n_{(nPop,j)} & n_{(nPop,nVar-1)} & n_{(nPop,nVar)} \end{bmatrix} \quad (9)$$

where, $n_i^{(t)}$ denote a set of current solutions. This position vector can be generated using the lower and upper boundary conditions defined for the control variable in Equation (10):

$$n_{i,j}^{(t)} = r_1 \times (ub_j - lb_j) + lb_j \quad (10)$$

where r_1 is a random integer produced within the range $[0, 1]$ and ub and lb are the upper and lower bounds for the control variables, respectively. The nominee solution ($nPop$) is subjectively assigned since there is no exact rule available for its estimation. The smell molecules diffused through Brownian motion towards the agent. For this diffusion, each molecule is assigned a velocity as in Equation (11)

$$w_i^{(t)} = \begin{bmatrix} W_{(1,1)} & \cdots & W_{(1,j)} & W_{(1,nVar-1)} & W_{(1,nVar)} \\ W_{(2,1)} & \cdots & W_{(2,j)} & \cdots & W_{(2,nVar)} \\ \cdots & \cdots & W_{(i,j)} & \cdots & \cdots \\ \vdots & \vdots & \vdots & \vdots & \vdots \\ W_{(nPop-1,1)} & \cdots & W_{(nPop-1,j)} & \cdots & W_{(nPop-1,nVar)} \\ W_{(nPop,1)} & \cdots & W_{(nPop,j)} & W_{(nPop,nVar-1)} & W_{(nPop,nVar)} \end{bmatrix} \quad (11)$$

The molecules employ the velocity vector in Equation (11) to update their initial position, as depicted in Equation (12)

$$n_i^{(t+1)} = n_i^{(t)} + w_i^{(t)} \quad (12)$$

Each molecule updates its location in the hyperspace according to Equation (13) continuously until it reaches the agent's static position:

$$n_i^{(t+1)} = n_i^{(t)} + n_i^{(t+1)} \quad (13)$$

where $w_i^{(t+1)}$ is the velocity update equation given by Equation (14)

$$w_i^{(t+1)} = w_i^{(t)} + r_2 \times \sqrt{\frac{3kT}{m}} \quad (14)$$

where k denotes the Boltzmann's constant, also refers to as the smell constant, m and T stands for the mass and temperature of smell molecules, respectively, while r_2 is a random value that penalizes the impact of the molecular characteristics on the smell velocity.

The updated molecules position given in Equation (15), represents the sniffing mode of the SAO algorithm. The fitness of this mode is evaluated, and the molecules with the best nominee solution is elected as the agent donated by $n_{agent}^{(t)}$. In the same manner, the molecule with the worst sniffing fitness is determined, and this molecule is represented as $n_{worst}^{(t)}$.

2.3.2 Trailing Mode

All the molecules in Equation (9) have a unique chance of becoming a smelling agent, depending on their initial positions. While searching the hyperspace, the assemblage of smell molecules may become higher than the current nominee position of the agent. When this happens, the agent adopts this new position using its position ($n_{agent}^{(t)}$) and the position of molecules with the worst fitness ($n_{worst}^{(t)}$) is derived from the sniffing mode. This movement is achieved using Equation (15):

$$n_i^{(t+1)} = n_i^{(t)} + r_3 \times olf \times (n_{agent}^{(t)} - n_i^{(t)}) - r_4 \times olf \times (n_{worst}^{(t)} - n_i^{(t)}) \quad (15)$$

where r_3 and r_4 are numbers generated randomly in the range of [0,1] to penalize the effect of olfaction capacity (olf) on ($n_{agent}^{(t)}$) and ($n_{worst}^{(t)}$) respectively. It is important to note that the $n_i^{(t)}$ in Equation (15) is the position of the updated molecule obtained from the sniffing mode. Realistically, the agent should be able to sniff the smell molecules and intuitively follow these molecules confidentially until it is identified. This usually bemuses the

agent due to variation in mass and temperature of smell molecules and variation in the *olf*. To mitigate this limitation, the agent adopts a random search strategy called the random mode.

2.3.3 The Random mode

If the trailing mode fails to achieve the global solution, the agent will use the random mode to escape being caught in local minima. The random mode is implemented using Equation (16).

$$n_i^{(t+1)} = n_i^{(t)} + r_5 \times step \quad (16)$$

where *step* is a constant step size assigned arbitrarily, r_5 denotes the random number within the range (0,1] and $n_i^{(t)}$ is the molecule's position obtained from trailing mode. The influence of the random mode becomes significant if the sniffing and the trailing modes fail to attain global fitness. If this happens, the agent takes a constant step movement in the hyperspace using the random mode. Three major assumptions necessary to implement the SAO are given in the literature [27]. Figure 7 is a flowchart of the standard SAO. The process starts with the initialization and then the sniffing mode and gradually switches to other modes based on comparison and updating the fitness, agents and worst molecules until the optimal solution is found. The SAO program is created and simulated in MATLAB/SIMULINK.

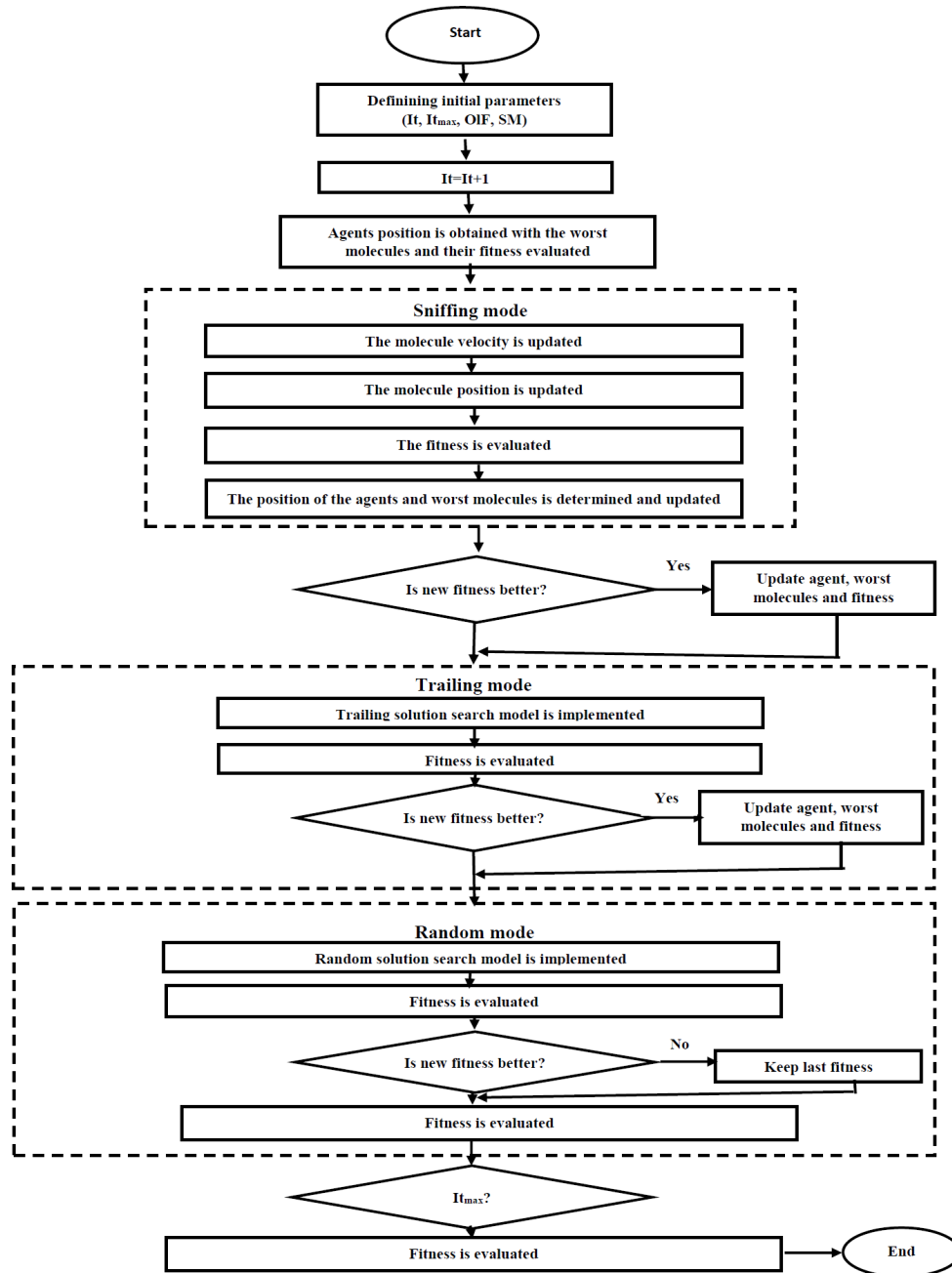


Figure 7: SAO (FE =number of function evaluations, SM = small molecules, Itr =Iteration, Itr_{max} =maximum iteration)

2.4 Optimal sizing of the HRES using the SAO

Three HRESs, i.e. wind/battery, PV/wind/battery, and PV/battery scheme, were taken into account in this study, and the two novel algorithms (i.e QOBL-SAO and the LFQOBL-SAO) will be utilized to find the best possible mix of RES that meets the energy demand. The following are the objective system formulation and constraints utilized in the design of HRES.

2.4.1 Objective system formulation

The goal of this study is to minimize the Excess Energy (EE), LPSP and LCE generated through a tri-objective optimization problem. The individual objective functions can be expressed in Equations (17)-(19):

$$LCE = \frac{C_{A_total}}{E_{total}} \quad (17)$$

$$LPSP = \frac{\sum_0^T P_{Load} - P_{pv} - P_{wind} - P_{SOC_M}}{\sum_0^T P_{Load}} \quad (18)$$

$$EE = \sum_0^T \frac{P_{Load} - P_{pv} - P_{wind}}{\sum_0^T P_{Load}} \quad (19)$$

where C_{A_tot} represents the total cost of the HRES, E_{total} represents the total cost of energy generation, P_{SOC_M} shows the amount of power discharged by the battery storage system and T represents the total time. The equations for determining P_{pv} and P_{wind} can be found in the literature[37][38].

The total annualized cost (TAC) given in Equation (20) must also be minimized to achieve the tri-objective.

$$TAC = \sum_{i=1}^N AMC + \sum_{i=1}^N ACC \quad (20)$$

where N stands for the overall number of hours considered, ACC for annualized capital cost, and AMC for the annual maintenance. The AMC is calculated using Equation (21):

$$AMC = n_{pv}P_{pv} + n_{wt}P_{wt} \quad (21)$$

The ACC , on the other hand, is calculated using Equation (22) as follows:

$$ACC = CFR \times [n_{pv}C_{pv} + n_{wt}C_{wt} + n_{Bat}C_{Bat} + n_{Inv}C_{Inv}] \quad (22)$$

where n_{pv} , n_{wt} , n_{Bat} , n_{Inv} represents the number of PV, wind turbine, batteries and converter respectively, while C_{pv} , C_{wt} , C_{Bat} and C_{Inv} denote the unit costs of the PV, wind turbine, batteries and converter, respectively. CRF is the Capital Recovery Factor.

In this study, it is intended to design three schemes for a healthcare facility at Jibia, i.e. Wind/Battery, PV/Wind/Battery and PV/Battery. To obtain the AMC for the PV/battery systems (AMC_{pv}), equations (21) and (22) are modified to become equation (23):

$$AMC_{pv} = n_{pv}P_{pv} \quad (23)$$

whereas the total capital cost for the PV/battery (ACC_{PV}) is calculated using Equation (24):

$$ACC_{PV} = CFR \times [n_{pv}C_{pv} + n_{Bat}C_{Bat} + n_{Inv}C_{Inv}] \quad (24)$$

Similarly, the AMC for the wind/battery system (AMC_{wt}) is shown in equation (25):

$$AMC_{wt} = n_{wt}P_{wt} \quad (25)$$

Whereas the total capital cost for the wind/battery system (ACC_{wt}) is calculated using Equation (26)

$$ACC = CFR \times [n_{wt}C_{wt} + n_{Bat}C_{Bat} + n_{Inv}C_{Inv}] \quad (26)$$

The number of each hybrid component is chosen as a decision variable in all three configurations based on the boundary constraints of Equations (27)-(29):

$$n_{pv-max} \leq n_{pv} \leq n_{pv-min} \quad (27)$$

$$n_{wt-max} \leq n_{wt} \leq n_{wt-min} \quad (28)$$

$$n_{Bat-max} \leq n_{Bat} \leq n_{Bat-min} \quad (29)$$

where n_{pv-max} and n_{pv-min} are the maximum and minimum number of PV panels. Similarly the minimum and maximum number of wind turbines and batteries is given in Equations (28) and (29). For PV/Wind/Battery and the other two configurations, the number of inverters is set to four and three, respectively.

To achieve a reliable power supply, the system must satisfy the reliability constraint, which is given by Equation (30):

$$LPSP \leq \beta_g \quad (30)$$

where β_g is the system tolerance limit reliability. This strategy ensures that the battery is never completely depleted or overcharged. Equation (31) expresses the constraints.

$$SOC_{min} \leq SOC \leq SOC_{max} \quad (31)$$

3.0 Implementation of the optimum HRES based on the SAO

The steps involved in implementing the SAO is according to the flowchart in Figure 7, as follows:

- 1) The initial velocity (V), $nPop$, $nVar$, T , m , olf and the Itr parameters are defined. The problem dimension, in this case, are selected as 3, 2, and 1 depending on the hybrid configurations. 3 represents PV/wind/battery system, while 2 and 1 represent PV/battery and wind/battery systems, respectively.

- 2) Randomly generating an initial solution for the hybrid systems decision variables and allocating initial velocity to each solution.
- 3) Evaluating the fitness of each solution and determining the agent
- 4) Updating the velocity using the sniffing mode velocity.
- 5) Evaluating the fitness of the sniffing mode and updating the agent's position.
- 6) Determining the position of the molecules with the worst sniffing fitness and performing the trailing mode behavior.
- 7) Evaluating the fitness of the trailing mode described in step 6 above
- 8) Comparing the fitness of the trailing mode with the fitness obtained during the sniffing mode.
- 9) If the trailing mode fitness was better than that of the sniffing mode, then terminate the program.

The parameters of the QOBL-SAO and LFQOBL-SAO used to develop the HRES is given in Table 2.

Table 2: Simulation Parameters for the SAO

S/No	Parameter	Symbol	Value
1	Number of Population	$nPop$	50
2	Number of the Decision variable	$nVar$	3
3	Temperature	T	3
4	Mass	m	2.4
5	Step Length	SL	2.5
6	Boltzmann's Constant	k	1.38×10^{-23}
7	Maximum Iteration	Itr	100
8	Lower Bound	lb	[0,0,0]
9	Upper Bound	ub	[100, 100, 50]

3.1 Improvements of the SAO algorithms

In this study, two improved versions of the SAO have been developed, i.e. the Quasi oppositional based learning SAO (QOBL-SAO) and the levy flight-SAO (LFQOBL-SAO) and their results compared to the standard SAO. The QOBL-SAO utilizes quasi-opposition-based initialization and generation jumping [39]. In this case, by using the opposite points, improved initial conditions are obtained, referred to as the opposite population, even when no prior knowledge about the solutions exists. In reality, the QOBL-SAO tries to create the opposite of the initial population of smell agents in order to expand the parameters in the search space. To implement the QOBL-SAO, a function is created in MATLAB with the QOBL-SAO pseudocode, as shown in Algorithm 1. Out of the three

characteristics of the SAO, the random mode has a weak concept. The random mode just adds a random number to the initial population, and it does not help the algorithm converges faster. To overcome this problem, the LFQOBL-SAO is introduced to improve the weak nature of the random mode. The LFQOBL-SAO improves the performance and the search space[40]. Care has to be taken in implementing the LFQOBL-SAO because if the step is outsized, the improved solution could definitely exceed the true solution; However, if the step size is small, the convergence rate may decrease, resulting in an underperformance of the algorithm. In the LFQOBL-SAO algorithm, the random code is replaced by the levy flight function. The LFQOBL-SAO algorithm is shown in Algorithm 2.

ALGORITHM 1: PSEUDOCODE FOR THE QOBL-SAO

Inputs: N, d, preliminary population (x), L, U
Output:

```

1  for i = 1: N
2  | for j = 1: d
3  |    $x_{i,j}^o = L_j + U_j - x_{i,j}$  % creating the reverse of the present population
4  |    $D_{i,j} = (L_j + U_j)/2$ 
5  |   if  $(x_{i,j} < D_{i,j})$  % generating quasi opposite of x
6  |   |  $x_{i,j}^{qo} = D_{i,j} + (x_{i,j}^o - D_{i,j}) \times rand$ 
7  |   | else
8  |   |  $x_{i,j}^{qo} = D_{i,j} + (D_{i,j} - x_{i,j}^o) \times rand$ 
9  |   | end
10 |   end
11 End

```

[N= number of molecules, d= variables dimension, L and U are the settings for the minimum and maximum value of the initial population]

ALGORITHM 2: PSEUDOCODE OF THE LFQOBL-SAO

Input: $\min f(x)$, τ , β and σ_h
Output:

```

1  Select the population  $x_i$  to modify the position.
2  Compute  $\sigma_h$  update (from Equation 32)
3  while ( $\tau < \epsilon$ ) do
4  |   Compute step_size (from equation 33)
5  |   Generate New Solution  $x'_i$  (from equation 34)
6  |   Compute  $f(x'_i)$ 
7  |   if  $f(x_i) > f(x'_i)$  then
8  |   |    $x_i = x'_i$ 
9  |   | end if
10 | end while

```

[τ = is the step size]

Equations (32-34) are used to compute the respective parameters of the LFQOBL-SAO pseudocode.

$$\sigma_h = \left\{ \frac{\sin(\frac{\pi\beta}{2})\Gamma(1+\beta)}{2^{\frac{\beta-1}{2}}\beta\Gamma(\frac{1+\beta}{2})} \right\} \quad (32)$$

$$\text{Step_size}(\tau) = s(\tau) \times 0.01; \quad (33)$$

$$x'_i(\tau + 1) = x'_i(\tau) + \text{Step_size}(\tau) \times U(0,1) \quad (34)$$

4.0 The evaluation criteria for the QOBL-SAO and LFQOBL-SAO

In this section, improved versions of the SAO, i.e. the QOBL-SAO and the LFQOBL-SAO were evaluated using certain CEC benchmark functions. Before any new optimization approach is applied, some benchmark functions can be utilized to evaluate its performance. In this study, 10 of these functions with diverse features were chosen and categorized into three as follow; unimodal and separable functions (USF), multimodal and non-separable functions (NS), unimodal and nonseparable functions (NSF). One global optimum exists for unimodal functions, which aids in evaluating their exploitation potential of the SAO. Multimodal functions often have more than one local optimal point, which is useful for analyzing SAO's exploration potential. There is a single global optimum for unimodal functions, which is important for assessing the exploitation potential of the QOBL-SAO and LFQOBL-SAO. It is easier to investigate the exploratory potential of modified version of the SAO when dealing with multimodal functions because they have two or more local optimal points. These clusters are shown in further detail in Tables 3, 4, and 5. Table 3 provides benchmark functions in two dimensions from (A1) to (A5), Table 4 is the benchmark function in five dimension, i.e. (A6) and Table 5 shows the benchmark functions in thirty dimensions i.e (A7) to (A10) [41][42].

Table 3: The benchmark test functions for two dimensions

FNo	Name	D	Formula	C	Range	Fmin
A1	Bohachevsky1	2	$f(x) = 2x_2^2 + x_1^2 - 0.3\cos(3\pi x_1) - 0.4\cos(4\pi x_2) + 0.7$	NS, NSF	[-100, 100]	0
A2	Bukin F6	2	$f(x) = 0.01 x_1 + 10 + 100\sqrt{ x_2 - 0.01x_1^2 }$	NS, NSF	[-15, -3; - 3,3]	0
A3	Matyas	2	$f(x) = -0.48x_1x_2 + 0.26(x_1^2 + x_2^2)$	NS, USF	[-10,10]	0
A4	Schaffer	2	$f(x) = \sum_{i=1}^{30} \{[\sin 50(x_i^2 + x_{i+1}^2)^{0.1}]^2 + 1\}(x_i^2 + x_{i+1}^2)^{0.25}$	NS, NSF	[-100, 100]	0
A5	Styblinski-Tang	2	$f(x) = \frac{1}{2} \sum_{i=1}^n (5x_i + x_i^4 - 16x_i^2)$	NS, NSF	[-5, 5]	-78.332

Table 4: The benchmark functions for five dimensions

FNo	Name	D	Formula	C	Range	Fmin
A6	Michalewicz	5	$f(x) = - \sum_{i=1}^2 (\sin(ix_i^2/\pi))^{20} \sin(x_i)$	NS, NSF	[0, π]	- 4.6877

Table 5: The benchmark test functions for Thirty-dimensions

FNo	Name	D	Formula	C	Range	Fmin
A7	Ackley	30	$f(x) = -20 \exp\left[-\frac{1}{5} \sqrt{\frac{1}{n} \sum_{i=1}^D x_i^2} + 20\right]$ $+ \exp\left[\frac{1}{n} \sum_{i=1}^D \cos(2\pi x_i)\right] + e$	NS, NSF	[-32,32]	0
A8	Ellipsoid	30	$f(x) = \sum_{i=1}^n x_i^2 \cdot i$	NS, USF	[-5.12,5.12]	0
A9	Rastrigin	30	$f(x) = \sum_{i=1}^n [x_i^2 - 10 \cos(2\pi x_i)] + 10n$	NS, NSF	[-5.12,5.12]	0
A10	Salomon	30	$f(x) = +0.1 \sqrt{\sum_{i=1}^{30} x_i^2} + 1 - \cos\left(2\pi \sqrt{\sum_{i=1}^{30} x_i^2}\right)$	NS, NSF	[-100,100]	0

5.0 Analysis of Benchmark Functions Results

The accuracy of the LFQOBL-SAO and QOBL-SAO to the benchmark functions is covered in the first part, and the convergence analysis of the techniques is covered in the subsequent section

5.1 Solution Accuracy Study for CEC benchmarked functions

The statistical outcomes produced for each algorithm across 30 separate runs are reported based on the tests performed on the benchmark functions in Tables 3, 4 and 5. Table 6 displays the results for the 2D benchmark functions. Table 7 display the results for the 5D benchmark function, while Table 8 show the results for the 30D benchmark functions. Each algorithm's best, average, standard deviation and rank are displayed for each benchmark function. The LFQOBL-SAO and QOBL-SAO's performance is evaluated using the best values of the benchmark functions. The mean value or standard deviation is used to break ties when more than one algorithm yields the best result. If all g algorithms get the same best result in any of the benchmark functions, the top-performing algorithm after g is ranked g+1. The results from Tables 6,7 and 8 imply that the novel algorithms, i.e. QOBL-SAO and LFQOBL-SAO, are as good or better than the standard SAO algorithm. The convergence plots for the novel algorithms and the SAO are shown in Figure 8, based on some selected functions. The results shows that either of the the novel algorithms has lower fitness value than the SAO in all the functions considered.

Table 6: Comparison results for 5 2D Benchmark functions

Functions	Performance metric	SAO	QOBL-SAO	LFQOBL-SAO
A1	Average	6.45527	0.0012285	0.0107181
	Best	0.05489	2.61×10^{-13}	1.67064×10^{-8}
	Standard deviation	44.5398	0.008686	0.0587
	Rank	3	1	2
A2	Average	5.1049	3.6529	2.2018
	Best	5.097	3.6126	2.130956
	Standard deviation	0.0577	0.24396	0.38817
	Rank	3	2	1
A3	Average	0.0030462	3.62×10^{-12}	7.6385
	Best	7.416×10^{-6}	5.219×10^{-16}	1.595×10^{-12}
	Standard deviation	0.0212	2.529	0.0041837
	Rank	3	1	2
A4	Average	3.54×10^{-4}	7.4066×10^{-7}	2.58316×10^{-4}
	Best	4.0118×10^{-12}	1.85×10^{-14}	6.4192×10^{-11}
	Standard deviation	0.00252744	5.23×10^{-96}	0.001414
	Rank	2	1	3
A5	Average	-78.1365	-78.33	-78.1249
	Best	-78.3318	-78.1166	-78.3323
	Standard deviation	1.37988	1.5239	1.1352
	Rank	2	3	1

Table 7: Results in 5D

Functions	Performance metric	SAO	QOBL-SAO	LFQOBL-SAO
A6	Average	-4.9997	-4.9997	-4.9988
	Best	-4.999	-4.999	-4.999
	Standard deviation	0.00142	0.001598	0.00613783
	Rank	1	2	3

Table 8: Comparison of 30D Benchmark Functions

Functions		SAO	QOBL-SAO	LFQOBL-SAO
A7	Average	0.127655	0.0058	0.0038
	Best	0.014448	9.28×10^{-8}	5.19×10^{-5}
	Standard deviation	0.5738	0.00474	0.02049
	Rank	3	1	2
A8	Average	4.4760	1.7887×10^{-5}	1.2366×10^{-5}
	Best	2.6697×10^{-12}	1.6423×10^{-18}	1.198×10^{-12}
	Standard deviation	0.003165	1.264×10^{-6}	6.7734×10^{-5}
	Rank	3	1	2
A9	Average	6.0433×10^{-4}	1.065×10^{-13}	3.364×10^{-9}
	Best	0.05729	2.716×10^{-5}	0.0409
	Standard deviation	0.3027	1.92×10^{-4}	0.22397
	Rank	3	1	2
A10	Average	0.013523	1.05453×10^{-7}	6.157×10^{-6}
	Best	0.04978	4.88×10^{-5}	0.00939
	Standard deviation	0.10179	3.442×10^{-4}	0.0512
	Rank	3	1	2

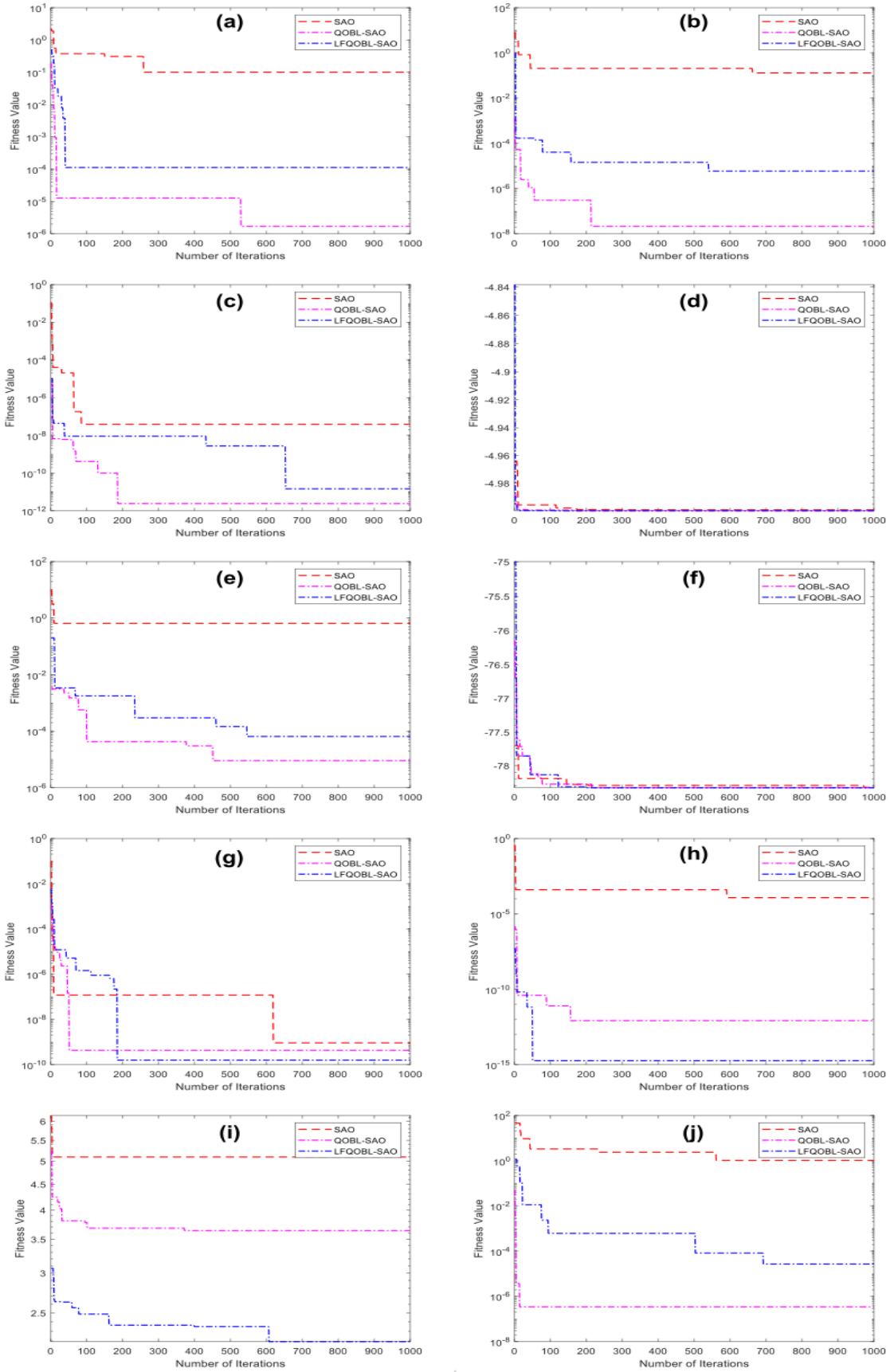


Figure 8: Convergence plots (Minimum fitness values) for the SAO, QOBL-SAO and LFQOBL-SAO based on some selected CEC benchmarked functions a) A10 b) A9 c) A8 d) A6 e) A7 f) A5 g) A4 h) A3 i) A2 and j) A1

5.2 Solution Accuracy Study for CEC2020 Real world constrained optimization competition

To better understand the robustness of the proposed LFQOBL-SAO and QOBL-SAO, they are applied to solve the CEC2020 real world constrained optimization competition problems and their results are compared to top performing algorithms such as the IUDE, MAgES, and iLSHADε. The selected optimization problems of the CEC2020, are described below

5.2.1 Process synthesis problem:

This problem contains no linear variables, either real or binary. The goal of this problem is to find the minimum value of the following function using Equation (35):

$$f(\bar{m}) = (1 - m_4)^2 + (1 - m_5)^2 + (1 - m_6)^2 - \ln(1 + m_7) + (1 - m_1)^2 + (2 - m_2)^2 + (3 - m_3)^2 \quad (35)$$

subject to certain constraints and bounds[43].

5.2.2 Weight minimization of a speed reducer:

In this case, the creation of a speed reducer for a small aircraft engine is involved. The optimization problem takes the form of equation (36):

$$f(\bar{m}) = 0.7854m_2^2m_1(14.9334m_3 - 43.0934 + 3.333333m_3^2) + 0.7854(m_5m_7^2 + m_4m_6^2) - 1.508m_1(m_7^2 + m_6^2) + 7.477(m_7^3 + m_6^3) \quad (36)$$

subject to certain constraints and bounds[44]

5.2.3 Tension/compression spring design:

The weight of a tension or compression spring must be optimized as the main goal of this problem. The definition of the problem is provided in Equation (37):

$$f(\bar{m}) = m_1^2 + m_2(2 + m_3) \quad (37)$$

subject to certain constraints and bounds [45].

5.2.4 Three-bar truss design problem:

This optimization problem, which has an accidental space constraint, is taken from civil engineering, with the goal of reducing the weight of the bar structures. The stress constraints of each bar serve as the basis for this problem's constraints. Three non-linear constraints and a linear objective function characterize the resulting problem. Its mathematical description is given in Equation (38):

$$f(\bar{m}) = (m_2 + 2\sqrt{2}m_1) \quad (38)$$

subject to certain constraints and bounds[46]

5.2.5 Design of gear train:

The main goal of this problem is to reduce the gear ratio needed to arrange the compound gear train. The ratio of the angular velocities of the output and input shafts is used to describe the gear train ratio. The problem aims to minimize the following function presented in Equation (39):

$$f(\bar{x}) = \left(\frac{1}{6.931} - \frac{m_1 m_2}{m_3 m_4} \right) \quad (39)$$

Subject to certain constraints and bounds[47]

Table 9 compared the performance of the LFQOBL-SAO, QOBL-SAO and SAO with some top performing CECE2020 algorithms. It is obvious the LFQOBL-SAO and QOBL-SAO are capable of solving real time engineering problems. When compared with the best known feasible objective function value in the literature [48], the results of the the LFQOBL-SAO and QOBL-SAO are very much closer to the possible solutions and are as good as the IUDE, εMAGES, and iLSHAdε algorithms[48].

6.0 Results Obtained Using the SAO and its modified versions

The results of the three scenarios, wind/battery, PV/wind/battery, and PV/battery, evaluated using the SAO, QOBL-SAO, and LFQOBL-SAO, are presented and compared in this section. For each configuration, a total of thirty independent runs were conducted.

Table 9: Comparison of CEC2020 Benchmark Functions

Functions	Performance metric	SAO	QOBL-SAO	LFQOBL-SAO	IUDE	ϵ MAgES	iLSHAD ϵ
Process synthesis problem	Average	1.43	1.9698	1.8919	2.00	1.99	2.00
	Best	1.59	2.0184	2.00087	2.00	2.00	2.00
	worst	1.29	1.611	1.433	2.00	1.29	2.00
	Standard deviation	0.073125	0.10237	0.1948	6.41×10^{-17}	0.152	0
Weight minimization of a speed reducer	Average	3.11×10^3	3.03×10^3	3.13×10^3	2.99×10^3	2.99×10^3	2.99×10^3
	Best	3.034×10^3	3×10^3	3.069×10^3	2.99×10^3	2.99×10^3	2.99×10^3
	worst	3.1925×10^3	3.069×10^3	3.21×10^3	2.99×10^3	2.99×10^3	2.99×10^3
	Standard deviation	43	14.98	37	4.64×10^{-13}	4.64×10^{-13}	4.64×10^{-13}
Tension/compression spring problem	Average	0.02126	0.01396	0.097027	0.0127	0.0127	0.013
	Best	0.01329	0.0129	0.013244	0.0127	0.0127	0.0127
	worst	0.0339	0.0255	0.054476	0.0127	0.0137	0.0178
	Standard deviation	0.00616	0.002606	0.1288	1.08×10^5	2.16×10^{-4}	1.06×10^{-3}
Three bar truss design problem	Average	2.63×10^2	2.639×10^2	2.6395×10^2	2.64×10^2	2.65×10^2	2.64×10^2
	Best	2.63×10^2	2.638×10^2	2.64×10^2	2.64×10^2	2.64×10^2	2.64×10^2
	worst	2.64×10^2	2.639×10^2	2.639×10^2	2.64×10^2	2.74×10^2	2.64×10^2
	Standard deviation	0.0434	0.003974	0.04345	0	2.88	1.99
Design of gear train	Average	5.088×10^{-8}	1.82×10^{-9}	1.599×10^{-7}	4.55×10^{-16}	0	5.56×10^{-17}
	Best	3.0675×10^{-10}	2.7×10^{-12}	3.299×10^{-9}	0	0	0
	worst	4.755×10^{-7}	8.7×10^{-9}	5.193×10^{-7}	8.41×10^{-15}	0	3.91×10^{-16}
	Standard deviation	9.744×10^{-8}	2.2×10^{-9}	1.996×10^{-7}	1.66×10^{-15}	0	1.17×10^{-16}

6.1 Optimisation convergence for SAO, QOBL-SAO and LFQOBL-SAO

This section discusses the outcomes of the optimization of the PV/battery, PV/wind/battery and Wind/battery systems for Jibia, Nigeria, using the SAO, QOBL-SAO, and LFQOBL-SAO optimization. In Figure 9, the convergence rates of SAO and its variants are compared for three different schemes, i.e. wind/battery, PV/wind/battery, and PV/battery schemes. The convergence rates show the iterations point at which the value of the objective function (i.e. TAC) does not vary. The SAO converged faster than the others for the wind/battery system and PV/wind/battery system, with approximately 44 and 15 runs, respectively. The SAO is faster in convergence because of its less complexity compared to the others and the fact that PV/wind/battery and the wind/battery are more complex systems to analyze than the PV/wind battery. This is most likely due to the variable nature of wind speed as well as the high cost of wind turbines. The LFQOBL-SAO has shown faster convergence in the PV/battery system. The LFQOBL-SAO has the lowest TAC for the PV/wind/battery scheme, whereas the QOBL-SAO has the lowest TAC for the PV/wind system. Although the SAO shows faster convergence, generally, it is not having the lowest TAC in all the three RE schemes.

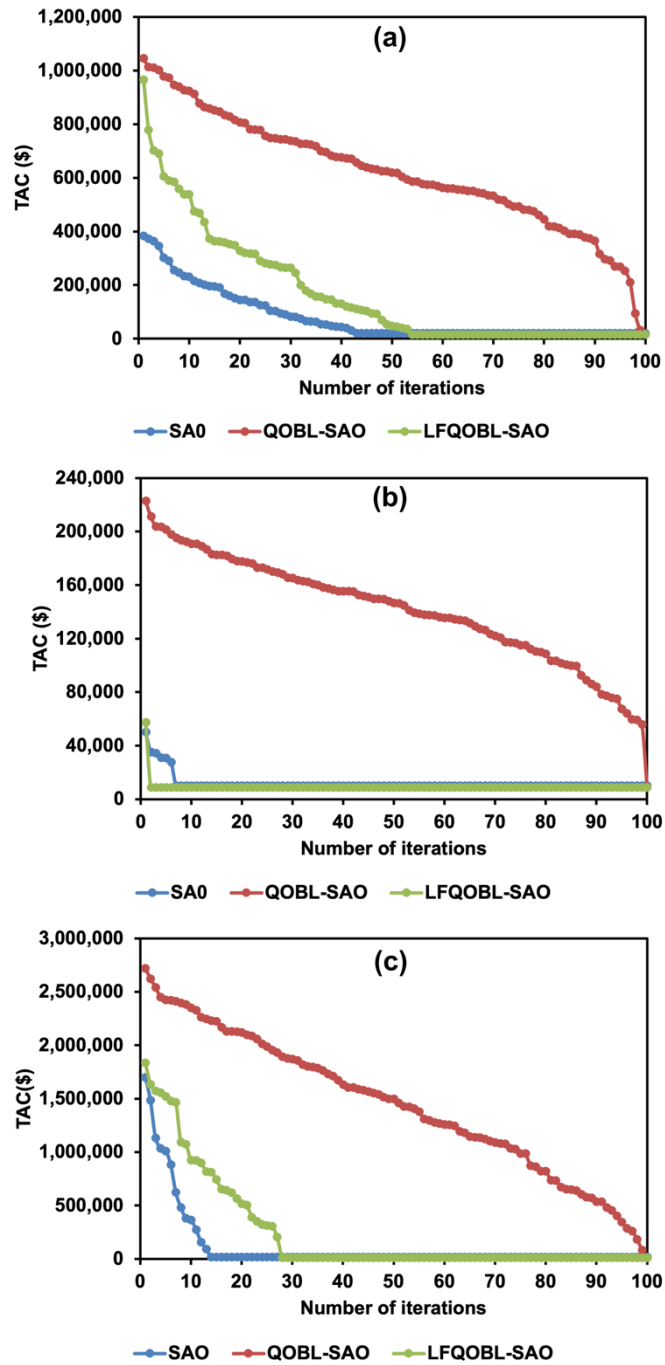


Figure 9: Convergence of characteristics of SAO, QOBL-SAO and LFQOBL-SAO for a) PV/wind/battery system b) PV/battery system and c) Wind/battery system.

6.2 Results analysis of HRES

The results of sizing HRES are provided and evaluated in this section. The HRES was designed using the parameters shown in Table 2. Each decision variable's lower and upper bounds (n_{pv} , n_{wt} , and n_{bat}) were set to 1 and 100, except the battery which has an upper bound of 50. The performance of the hybrid system results for the

three different renewable resource combinations is shown in Table 10. In the first instance, PV/Wind/Battery system is taken into consideration; in the second, battery and PV system (PV/battery) is considered. On the other hand, the third combination analyzes the Wind/battery system. The hybrid system would considerably reduce the possibility of no wind or solar output, making the system more dependable.

According to Table 10, the PV/Wind/Battery scheme is the most cost-effective way to meet the load demand requirements, using the QOBL-SAO and LFQOBL-SAO based approaches. The SAO and QOBL-SAO recorded TACs of \$20120 and \$15120, respectively, but the TAC of the PV/Wind/Battery system obtained by LFQOBL-SAO is \$15100. LFQOBL-SAO's optimal sizing for each scenario is as follows: PV/Wind/Battery: $n_{pv} = 51$, $n_{wt} = 33$, $n_{batt} = 20$, $n_{conv} = 4$; PV/Battery: $n_{pv} = 50$, $n_{wt} = 0$; $n_{batt} = 25$, $n_{conv} = 3$; Wind/Battery: $n_{pv} = 0$, $n_{wt} = 42$; $n_{batt} = 24$, $n_{conv} = 3$. The results imply that increasing the search space in the LFQOBL-SAO leads to a lower TAC of the three hybrid schemes. However, for the PV/battery and the wind/battery schemes, the LFQOBL-SAO has the lowest TAC, although SAO is slightly higher. In order to evaluate each algorithm's performance precisely, the average, best and standard deviation of each algorithm are provided in Table 11. For the SAO and LFQOBL-SAO, the TAC has been very consistent over several runs, which is not the case for the QOBL-SAO. The results imply that SAO and LFQOBL-SAO are more reliable algorithms for different combinations of RE schemes.

To determine the economic feasibility and adoption potential of the proposed hybrid systems, the LPSP and LCE for each hybrid system combination is determined (Table 12). The LPSP assists in determining when the energy produced will not be sufficient enough to satisfy the consumer demand. Any hybrid system will perform better if the LPSP is as close as possible to zero. To aid in the recovery of the hybrid system's cost over its lifetime, the LCE is used to calculate the average revenue per unit of the energy generated. In terms of LCE output, the QOBL-SAO technique appears to be the most cost-effective for all three hybrid schemes, though the LFQOBL-SAO technique is also cost-effective for the PV/battery scheme. The LPSP also shows that for all three schemes, the LFQOBL-SAO and QOBL-SAO provided more stable energy. The average excess energy/deficit for each technique also revealed that for all hybrid RE configurations, all sizing procedures yielded either excess energy or unmet energy. The excess energy in the hybrid schemes might be regarded as an undesirable scenario since it is wasted. The usage of a dump load might be an option for reducing the waste. The SAO has more excess energy than the others, while there exists unmet energy for the LFQOBL-SAO or QOBL-SAO schemes. Unmet energy is still acceptable for a certain period of the day. The cost implication of deploying any of the hybrid schemes with the three SAO algorithms is shown in Figures 10–12. Wind/Battery, PV/Wind/Battery, and PV/Battery systems' average component costs are denoted by the letters a, b, and c, respectively. The results provided in this

study will assist policymakers in determining the most cost-effective system for the healthcare facility at Jibia, Nigeria.

Table 10: Summary of results obtained by the three algorithms

Configurations	Sizing results	SAO	QOBL-SAO	LFQOBL-SAO
PV/Wind/battery system	NPV	100	33	51
	NWT	54	35	33
	NBAT	35	26	20
	CONV/INV	4	4	4
	PV cost (\$)	3.202×10^3	1.56×10^3	1.633×10^3
	WT cost (\$)	7.489×10^3	4.854×10^3	4.57×10^3
	Battery cost (\$)	8.69×10^2	6.456×10^2	4.966×10^2
	Converter/Inverter Cost (\$)	5.676×10^2	5.67×10^2	5.676×10^2
Total cost (\$)	2.012×10^4	1.512×10^4	1.51×10^4	
PV/Battery	NPV	100	60	50
	N _{WT}	0	0	0
	N _{BAT}	19	26	25
	N _{INV/CONV}	3	3	3
	PV cost (\$)	3.202×10^3	1.9217×10^3	1.6×10^3
	WT cost(\$)	0	0	0
	Battery cost(\$)	4.718×10^2	6.4566×10^2	6.208×10^2
	Converter/Inverter Cost(\$)	4.257×10^2	4.257×10^2	4.25×10^2
Total cost(\$)	1.01×10^4	8.99×10^3	8.647×10^3	
Wind/ Battery	N _{PV}	0	0	0
	N _{WT}	100	46	42
	N _{BAT}	20	23	24
	N _{INV/CONV}	3	3	3
	PV cost (\$)	0	0	0
	WT cost(\$)	1.3869×10^4	6.379×10^3	5.825×10^3
	Battery cost(\$)	4.966×10^2	5.711×10^2	5.96×10^2
	Converter/Inverter Cost(\$)	4.25×10^2	4.257×10^2	4.257×10^2
Total cost(\$)	2.079×10^4	1.3376×10^4	1.284×10^4	

Table 11: The average, standard deviation, best performances of the algorithm

Renewable system	Index	SAO (\$)	QOBL-SAO (\$)	LFQOBL-SAO(\$)
PV/wind/battery	Best	2.012×10^4	1.512×10^4	1.51×10^4
	Average	1.775×10^2	2.7711×10^5	1.5274×10^4
	Standard deviation	1.4699×10^{-11}	2.378×10^5	1.2862×10^{-11}
PV/battery	Best	1.01×10^4	8.99×10^3	8.647×10^3
	Average	1.01×10^4	1.2573×10^5	8.64×10^3
	Standard deviation	1.102×10^{-11}	6.68×10^4	9.187×10^{-12}
Wind/battery	Best	2.079×10^4	1.3376×10^4	1.284×10^4
	Average	2.078×10^4	-1.95×10^5	1.284×10^4
	Standard deviation	1.1024×10^{-11}	1.5077×10^5	0

Table 12: Reliability and Economic Analysis of Hybrid System

Renewable system	Index	SAO	QOBL-SAO	LFQOBL-SAO
PV/wind/battery	LCE (\$/kWh)	0.0395	1.75×10^{-4}	0.0025
	LPSP	0.04106	4.32×10^{-5}	4.038×10^{-5}
	Excess Energy(kW)	1.775×10^2	2.5428	1.8835
PV/battery	LCE (\$/kWh)	0.0332	0	0
	LPSP	0.0416	8.188×10^{-5}	8.188×10^{-5}
	Excess Energy(kW)	1.35×10^2	8.99	8.96
Wind/battery	LCE (\$/kWh)	0.01717	3.74×10^{-4}	0.003251
	LPSP	0.04106	5.925×10^{-5}	1.284×10^4
	Excess Energy(kW)	76	6.17	4.85

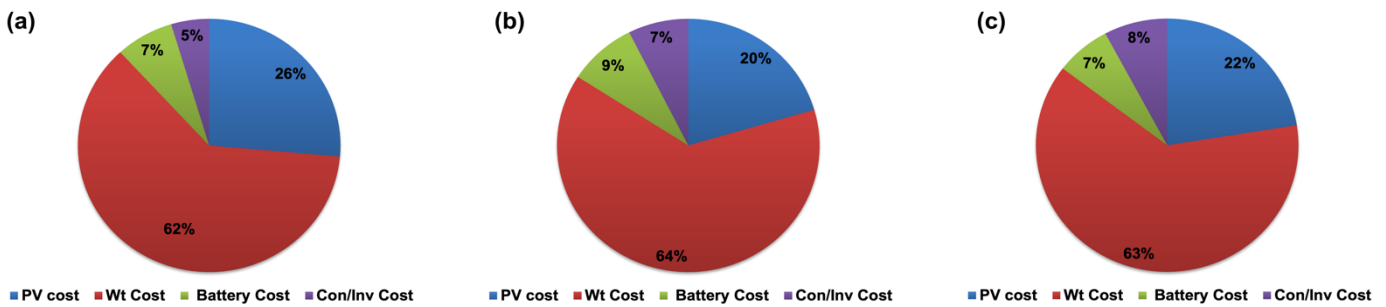


Figure 10: Percentage cost contribution for each component of the PV/Wind/battery system a) SAO b) QOBL-SAO c) LFQOBL-SAO

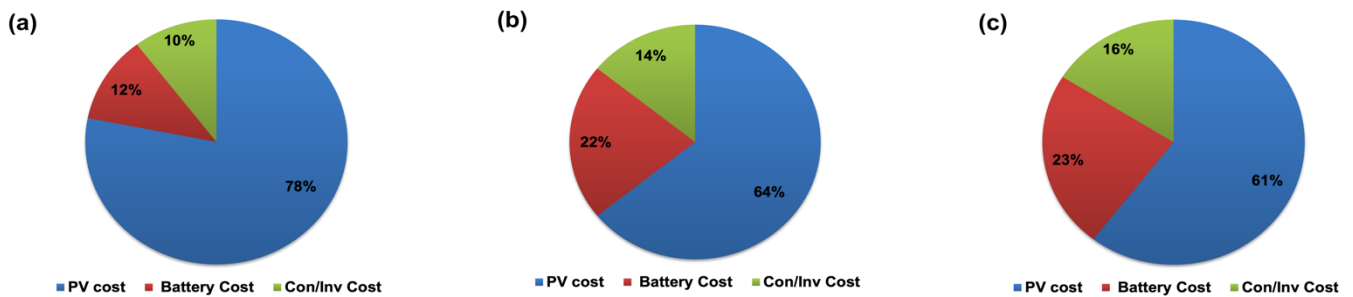


Figure 11: Percentage cost contribution for each component of the PV/Battery system a) SAO b) QOBL-SAO c) LFQOBL-SAO

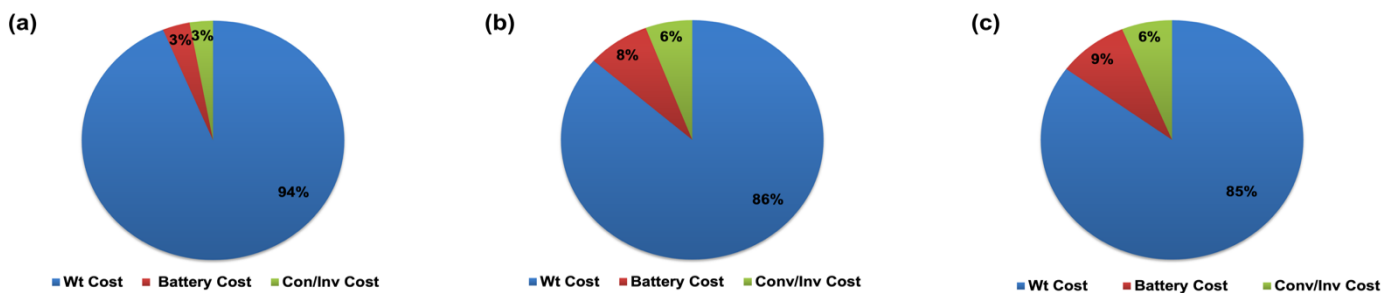


Figure 12: Percentage cost contribution for each component of the Wind/Battery system a) SAO b) QOBL-SAO c) LFQOBL-SAO

7.0 Conclusion:

This paper proposed two novel optimization techniques, i.e. QOBL-SAO and LFQOBL-SAO algorithms. First, they were evaluated on specific benchmarked functions and the CEC2020 real world optimization competition and the results compared with the SAO. Second, they are applied to find the optimum design of PV/wind/battery, PV/battery, and wind/battery systems. The results show that they have a global minimum on most of the CEC functions considered and are capable of solving the CEC2020 real world optimization competition. They can also optimize the hybrid scheme effectively. The LFQOBL-SAO algorithm has higher convergence and minimum TAC as compared to the QOBL-SAO and the SAO. This is because of more search space for the algorithm to converge in the LFQOBL-SAO. However, for the 25-year project lifetime, as demonstrated by the LCE, the QOBL-SAO appears to be the most economical. The LPSP also demonstrated that the LFQOBL-SAO and QOBL-SAO delivered a reliable energy for all three schemes. The LFQOBL-SAO and QOBL-SAO have shown less excess energy than the conventional SAO. Furthermore, the PV/wind/battery scheme is the most cost-effective scheme when the LFQOBL-SAO and QOBL-SAO are used. Generally, the results show that the proposed algorithms outperformed the standard SAO scheme.

Future work will focus on improving and refining the LFQOBL-SAO and QOBL-SAO algorithms through the use of additional optimization techniques, hybrid approaches, or integrating machine learning algorithms to improve their performance and efficiency. The scalability of the LFQOBL-SAO and QOBL-SAO algorithms for larger-scale HRES and other engineering optimization problems can also be investigated. Their convergence behaviour can also be studied as the system size and complexity increases, taking into account various factors such as multiple renewable sources, diverse load profiles, and dynamic operating conditions. Other areas of future studies include carrying out the sensitivity analysis of the QOBL-SAO and LFQOBL-SAO to evaluate their robustness to changes in input parameters, system configurations, and optimization objectives. This analysis can provide insights into the algorithms' performance under different scenarios and help identify the critical factors affecting their effectiveness. One possible limitation of the present study is the lack of validation of the LFQOBL-SAO and QOBL-SAO algorithms using real-world data and case studies from existing HRES. There is also need to conduct economic and policy analysis to assess the financial viability and policy implications of implementing optimized HRES. Certain factors, such as government incentives, tariff structures, market dynamics, and

regulatory frameworks, should be considered to provide a comprehensive assessment of the scheme's practical implications, and they can provide better managerial insights to practically implementing the scheme.

Acknowledgement

The authors wish to acknowledge the support provided by Jubail Industrial college in providing the facilities to conduct the research.

Reference

- [1] Abubakar Mas'ud A. Comparison of three machine learning models for the prediction of hourly PV output power in Saudi Arabia. *Ain Shams Eng J* 2022;13:101648. <https://doi.org/10.1016/J.ASEJ.2021.11.017>.
- [2] Li J, Liu P, Li Z. Optimal design and techno-economic analysis of a solar-wind-biomass off-grid hybrid power system for remote rural electrification: A case study of west China. *Energy* 2020;208. <https://doi.org/10.1016/J.ENERGY.2020.118387>.
- [3] Nadjemi O, Nacer T, Hamidat A, Salhi H. Optimal hybrid PV/wind energy system sizing: Application of cuckoo search algorithm for Algerian dairy farms. *Renew Sustain Energy Rev* 2017;70:1352–65. <https://doi.org/10.1016/J.RSER.2016.12.038>.
- [4] Bouchekara HREH, Sha'aban YA, Shahriar MS, Ramli MAM, Mas'ud AA. Wind farm layout optimisation considering commercial wind turbines using parallel reference points, radial space division and reference vector guided EA-based approach. *Energy Reports* 2023;9:4919–40. <https://doi.org/10.1016/J.EGYR.2023.04.014>.
- [5] Safari A, Jafari S, Assadi M. Role of gas-fuelled solutions in support of future sustainable energy world; Part I: Stimuluses, enablers, and barriers. *Green Energy Technol* 2018;0:1–33. https://doi.org/10.1007/978-981-10-8393-8_1.
- [6] Manoj Kumar N, Chopra SS, Chand AA, Elavarasan RM, Shafiullah GM. Hybrid Renewable Energy Microgrid for a Residential Community: A Techno-Economic and Environmental Perspective in the Context of the SDG7. *Sustain* 2020, Vol 12, Page 3944 2020;12:3944. <https://doi.org/10.3390/SU12103944>.
- [7] Haratian M, Tabibi P, Sadeghi M, Vaseghi B, Poustdouz A. A renewable energy solution for stand-alone power generation: A case study of KhshU Site-Iran. *Renew Energy* 2018. <https://doi.org/10.1016/j.renene.2018.02.078>.
- [8] Al-falahi MDA, Jayasinghe SDG, Enshaei H. A review on recent size optimization methodologies for standalone solar and wind hybrid renewable energy system. *Energy Convers Manag* 2017;143:252–74. <https://doi.org/10.1016/J.ENCONMAN.2017.04.019>.
- [9] Zhang G, Xiao C, Razmjoooy N. Optimal operational strategy of hybrid PV/wind renewable energy system using homer: a case study. <https://doi.org/10.1080/01430750.2020.1861087>.
- [10] Ekren O, Ekren BY. Size optimization of a PV/wind hybrid energy conversion system with battery storage using simulated annealing. *Appl Energy* 2010;87:592–8. <https://doi.org/10.1016/J.APENERGY.2009.05.022>.
- [11] Rajkumar RK, Ramchandaramurthy VK, Yong BL, Chia DB. Techno-economical optimization of hybrid pv/wind/battery system using Neuro-Fuzzy. *Energy* 2011;36:5148–53.

- <https://doi.org/10.1016/J.ENERGY.2011.06.017>.
- [12] Li J, Wei W, Xiang J. A Simple Sizing Algorithm for Stand-Alone PV/Wind/Battery Hybrid Microgrids. *Energies* 2012, Vol 5, Pages 5307-5323 2012;5:5307–23. <https://doi.org/10.3390/EN5125307>.
- [13] Al-Turjman F, Qadir Z, Abujubbeh M, Batunlu C. Feasibility analysis of solar photovoltaic-wind hybrid energy system for household applications. *Comput Electr Eng* 2020;86. <https://doi.org/10.1016/J.COMPELECENG.2020.106743>.
- [14] Shaqour A, Farzaneh H, Yoshida Y, Hinokuma T. Power control and simulation of a building integrated stand-alone hybrid PV-wind-battery system in Kasuga City, Japan. *Energy Reports* 2020;6:1528–44. <https://doi.org/10.1016/J.EGYR.2020.06.003>.
- [15] Ansari MS, Jalil MF, Manaullah, Diwania S. Techno-Economic Analysis of Diesel/Wind/PV/Battery Hybrid Energy System for Androth Island. *Lect Notes Electr Eng* 2021;723 LNEE:285–95. https://doi.org/10.1007/978-981-33-4080-0_27.
- [16] Frimpong SO, Agbehadji IE, Abayomi A, Millham RC, Freeman E, Ujakpa MM. Economic and reliability determination of sustainable renewable energy mix based on social spider prey optimization algorithm. vol. 8. Springer Berlin Heidelberg; 2023. <https://doi.org/10.1007/s00500-023-08231-8>.
- [17] Bhimaraju A, Ganesh GB, Mahesh A. Optimal Sizing of PV/Wind/Battery Stand-Alone Hybrid Renewable Energy Systems Using TLBO Algorithm 2023:65–73. https://doi.org/10.1007/978-981-19-9285-8_7.
- [18] Fu H, Shi M, Feng M. Capacity optimization strategy for energy storage system to ensure power supply. *Int J Low-Carbon Technol* 2023. <https://doi.org/10.1093/IJLCT/CTAD039>.
- [19] Izadyar N, Ong HC, Chong WT, Mojumder JC, Leong KY. Investigation of potential hybrid renewable energy at various rural areas in Malaysia. *J Clean Prod* 2016;139:61–73. <https://doi.org/10.1016/J.JCLEPRO.2016.07.167>.
- [20] Modu B, Aliyu A, Bukar AL, Abdulkadir M, Gwoma Z, Mustapha M. Techno-Economic Analysis of Off-Grid Hybrid PV-Diesel-Battery System in Katsina State, Nigeria. *Arid Zo J Eng Technol Environ* 2018.
- [21] (PDF) Strategic Developments In Renewable Energy In Nigeria n.d. https://www.researchgate.net/publication/237284856_Strategic_Developments_In_Renewable_Energy_In_Nigeria (accessed September 30, 2021).
- [22] How is 100% renewable energy possible for Nigeria? 2014.
- [23] Ugwoke B, Gershon O, Becchio C, Corgnati SP, Leone P. A review of Nigerian energy access studies: The story told so far. *Renew Sustain Energy Rev* 2020;120:109646. <https://doi.org/10.1016/J.RSER.2019.109646>.
- [24] Olatomiwa L, Mekhilef S, Huda ASN, Ohunakin OS. Economic evaluation of hybrid energy systems for rural electrification in six geo-political zones of Nigeria. *Renew Energy* 2015;83:435–46. <https://doi.org/10.1016/J.RENENE.2015.04.057>.
- [25] Babatunde OM, Adedoja OS, Babatunde DE, Denwigwe IH. Off-grid hybrid renewable energy system for rural healthcare centers: A case study in Nigeria. *Energy Sci Eng* 2019;7:676–93. <https://doi.org/10.1002/ESE3.314>.
- [26] Mas’ud AA. An optimal sizing algorithm for a hybrid renewable energy system. *Int J Renew Energy Res* 2017;7.
- [27] Salawudeen AT, Mu’azu MB, Sha’aban YA, Adedokun AE. A Novel Smell Agent Optimization (SAO): An extensive CEC study and engineering application. *Knowledge-Based Syst* 2021;232:107486. <https://doi.org/10.1016/J.KNOSYS.2021.107486>.
- [28] KEDCO | Kano Electricity Distribution Company Plc n.d. <https://www.kedco.ng/about.html> (accessed April 8, 2022).
- [29] BM O, OD O, PE U, MS A. Evaluation of some global solar radiation models in selected locations in

- Northwest, Nigeria. *MOJ Sol Photoenergy Syst* 2017. <https://doi.org/10.15406/mojsp.2017.01.00001>.
- [30] Massi Pavan A, Vergura S, Mellit A, Lughì V. Explicit empirical model for photovoltaic devices. Experimental validation. *Sol Energy* 2017;155:647–53. <https://doi.org/10.1016/J.SOLENER.2017.07.002>.
- [31] Al Garni HZ, Abubakar Mas'ud A, Baseer MA, Ramli MAM. Techno-economic optimization and sensitivity analysis of a PV/Wind/diesel/battery system in Saudi Arabia using a combined dispatch strategy. *Sustain Energy Technol Assessments* 2022;53:102730. <https://doi.org/10.1016/J.SETA.2022.102730>.
- [32] Danang LNA, Hably A, Bacha S, Tran TQ, Pham MC. Optimal sizing of battery energy storage system for an islanded microgrid. *Proc IECON 2018 - 44th Annu Conf IEEE Ind Electron Soc* 2018:1899–903. <https://doi.org/10.1109/IECON.2018.8591391>.
- [33] Kerdphol T, Fuji K, Mitani Y, Watanabe M, Qudaih Y. Optimization of a battery energy storage system using particle swarm optimization for stand-alone microgrids. *Int J Electr Power Energy Syst* 2016;81:32–9. <https://doi.org/10.1016/J.IJEPES.2016.02.006>.
- [34] Wang X, Palazoglu A, El-Farra NH. Operational optimization and demand response of hybrid renewable energy systems. *Appl Energy* 2015;143:324–35. <https://doi.org/10.1016/J.APENERGY.2015.01.004>.
- [35] Badr O, Mohammed A, Brahim D. Optimization of the thermal performance of the Solar Water Heater (SWH) using stochastic technique. *Int J Renew Energy Res* 2018;8:1401–10. <https://doi.org/10.20508/IJRER.V8I3.7666.G7439>.
- [36] Salawudeen AT, Olaniyan AA, Olarinoye GA, Sikiru TH. Formulation and Optimization of Overcurrent Relay Coordination in Distribution Networks Using Metaheuristic Algorithms. *Commun Comput Inf Sci* 2021;1350:389–402. https://doi.org/10.1007/978-3-030-69143-1_30.
- [37] Ramli MAM, Boucekara HREH, Alghamdi AS. Optimal sizing of PV/wind/diesel hybrid microgrid system using multi-objective self-adaptive differential evolution algorithm. *Renew Energy* 2018;121:400–11. <https://doi.org/10.1016/J.RENENE.2018.01.058>.
- [38] Ramli MAM, Hiendro A, Boucekara HREH. Performance analysis of hybrid PV/diesel energy system in western region of Saudi Arabia. *Int J Photoenergy* 2014;2014. <https://doi.org/10.1155/2014/626251>.
- [39] Nama S, Saha AK. An ensemble symbiosis organisms search algorithm and its application to real world problems. *Decis Sci Lett* 2018;7:103–18. <https://doi.org/10.5267/J.DSL.2017.6.006>.
- [40] Amalina Mohd Rosli K, Mustafa Z, Yusof Y, Farhan Mohamad Mohsin M. Dengue Outbreak Prediction Using an Improved Salp Swarm Algorithm. *IOP Conf Ser Mater Sci Eng* 2020;769. <https://doi.org/10.1088/1757-899X/769/1/012031>.
- [41] Çelik E. A powerful variant of symbiotic organisms search algorithm for global optimization. *Eng Appl Artif Intell* 2020;87:103294. <https://doi.org/10.1016/J.ENGAPPAI.2019.103294>.
- [42] Saha S, Mukherjee V. A novel chaos-integrated symbiotic organisms search algorithm for global optimization. *Soft Comput* 2018;22:3797–816. <https://doi.org/10.1007/S00500-017-2597-4>.
- [43] Kocis GR, Grossmann IE. A modelling and decomposition strategy for the minlp optimization of process flowsheets. *Comput Chem Eng* 1989;13:797–819. [https://doi.org/10.1016/0098-1354\(89\)85053-7](https://doi.org/10.1016/0098-1354(89)85053-7).
- [44] Chew SH, Zheng Q. *Integral global optimization : theory, implementation, and applications* 1988:179.
- [45] Belegundu AD, Arora JS. A study of mathematical programming methods for structural optimization. Part I: Theory. *Int J Numer Methods Eng* 1985;21:1583–99. <https://doi.org/10.1002/NME.1620210904>.
- [46] OPTIMIZATION IN PRE-CONTRACT SHIP DESIGN n.d. <https://trid.trb.org/view/14541> (accessed December 1, 2022).
- [47] Sandgren E. Nonlinear Integer and Discrete Programming for Topological Decision Making in Engineering Design. *J Mech Des* 1990;112:118–22. <https://doi.org/10.1115/1.2912568>.

- [48] Kumar A, Wu G, Ali MZ, Mallipeddi R, Suganthan PN, Das S. A test-suite of non-convex constrained optimization problems from the real-world and some baseline results. *Swarm Evol Comput* 2020;56. <https://doi.org/10.1016/J.SWEVO.2020.100693>.